Original Research Communication

Increased expression of p22phox mediates airway hyperresponsiveness in an experimental model of asthma

Chandran Nagaraj PhD[1], Hans Michael Haitchi MD, PhD[2,3,4], Akos Heinemann MD[5], Peter H. Howarth MD, DM[3], Andrea Olschewski MD[1,6], Leigh M. Marsh PhD[1]*

[1]Ludwig Boltzmann Institute for Lung Vascular Research, Graz, Austria. [2]The Brooke Laboratory, Academic Unit of Clinical and Experimental Sciences, Faculty of Medicine, University of Southampton, Southampton, United Kingdom.[3]National Institute for Health Research (NIHR) Southampton Respiratory Biomedical Research Unit, University Hospital Southampton NHS Foundation Trust, Southampton, United Kingdom. [4]Institute for Life Sciences, University of Southampton, Southampton, United Kingdom. [5]Institute of Experimental and Clinical Pharmacology, Medical University of Graz, Graz, Austria. [6]Department of Physiology, Medical University of Graz, Graz, Austria

Corresponding Author

Dr. Leigh M.Marsh, Ludwig Boltzmann Institute for Lung Vascular Research, c/o ZMF, Stiftingtalstrasse 24, 8010 Graz, Austria.

Email: Leigh.marsh@lvr.lbg.ac.at Tel: +43 316 385 72911 Fax: +43 316 385 72058

Abbreviated Title: Elevated p22phox in asthma

Word count: 5558

Number of reference: 47

Number of greyscale illustrations: 4

Colour illustration: 3 (online 1 and hard copy 2)

Abstract

Aim: Chronic airway diseases such as asthma are associated with increased production of reactive oxygen species (ROS) and oxidative stress. Endogenous NADPH oxidases are a major source of superoxide in lung, but their underlying role in asthma pathology is poorly understood. We sought to characterize the involvement of NADPH oxidase in allergic asthma by studying the role of CYBA (p22phox) in human asthma and murine house dust mite (HDM)-induced allergic airway inflammation.

Results: Increased expression and localisation of p22-*PHOX* was observed in biopsies of asthmatic patients. HDM treated wild-type mice possessed elevated p22phox expression, corresponded with elevated superoxide production. p22phox knockout (KO) mice did not induce superoxide and were protected against HDM-induced goblet cell hyperplasia and mucus production and HDM-induced airway-hyperreactivity (AHR). IL-13 induced tracheal hyperreactivity and Signal transducer and activator of transcription (STAT)6 phosphorylation was attenuated in the absence of p22phox or catalase pretreatment.

Innovation: Our study identifies increased expression of p22phox in lungs of asthmatic patients and in experimental model. The induced AHR and mucus hypersecretion is result of an increased ROS from the p22phox dependent NADPH oxidase, which in turn activates STAT6 for the pathological feature of Asthma.

Conclusions: Together with the increased p22phox expression in lungs of asthmatic patients, these findings demonstrate a crucial role of p22phox dependent NADPH oxidase for the development of mucus hypersecretion and AHR in HDM-induced model of asthma. This suggests inhibition of functional NADPH oxidase by selective interference of p22phox might hold promising therapeutic strategy for the management of asthma.

Introduction

Asthma is a complex chronic inflammatory disease characterised by airway inflammation and remodelling, mucus hypersecretion and airway hyperresponsiveness (AHR)(8,32). Airway obstruction has a multifactorial basis and ultimately determines the clinical manifestation and severity of asthma. Structural alterations such as collagen deposition and smooth muscle hypertrophy/hyperplasia lead to increased airway wall thickness and consequently increased basal bronchial tone (12). Infiltration of inflammatory cells in particular eosinophils and T cells into the airways and the increased expression of Th2 cytokines (IL-4, 5, 13) lead to enhanced airway smooth muscle contraction manifested as AHR (10,36).

Inflammatory diseases such as asthma are often associated with an increase in endogenous reactive oxygen species (ROS) (14,31). Exposure to allergens and other stimulants has been shown to stimulate ROS production, which can lead to oxidative stress–induced cell damage and mitigate the physiological function of structural cells (48). NADPH oxidase and mitochondria are the major contributors of basal endogenous ROS generation in the lung. The NADPH oxidase family consists of one of the membrane bound cytochrome isoforms (NOX1–4), the adaptor protein cytochrome b-245, alpha polypeptide (Cyba, also known as p22phox) and additional cytosolic regulatory proteins. Here p22phox functions as an adaptor molecule permitting the assembly and function of the active NADPH oxidase and is therefore crucial for NADPH oxidase-derived ROS production (2,35). The NADPH oxidases are enzyme complexes that generate ROS in form of hydrogen peroxide or super oxide by transfer of electrons from NADPH to molecular oxygen. Assembly and activation of NADPH oxidase requires the translocation of the cytoplasmic p40phox, p47phox and p67phox subunits to the membrane-bound gp91phox and p22phox subunits. The expression and cellular localization of NADPH oxidase determines its function in various cell types. In phagocytic cells NADPH oxidase-derived ROS is critical for the elimination of invading bacteria via induction of the oxidative burst. In structural cells NADPH oxidase is involved in several cellular processes such as signal transduction,

differentiation and proliferation (6,38). In the pulmonary system the production of ROS from NADPH oxidase has been implicated in several diseases such as asthma, chronic obstructive pulmonary disease, fibrosis and pulmonary hypertension (16).

Currently, there is limited evidence available on the functional contribution of NADPH oxidase in asthma pathogenesis. Haplotype analysis has revealed the association of single nucleotide polymorphisms (SNPs) in p22phox with bronchial asthma (24). Recently an increased NOX4 expression has been observed in airway smooth muscle bundles and in isolated smooth muscle cells from asthmatic patients (44). Studies using animal models have however given conflicting results. In one study mice deficient in NOX2 displayed reduced allergic airway inflammation following OVA challenge (42), while other studies reported that NOX2 deficient mice exhibited the reverse phenotype with increased inflammation and airway hyperreactivity (3,4,27).

To delineate the role and characterize the involvement of ROS generating NADPH oxidase in allergic airway inflammation and remodelling we have utilised the house dust mite (HDM) model in mice defective in the key NADPH oxidase adaptor molecule p22phox. We hypothesized that the lack of p22phox will inhibit functional NADPH oxidase complex thereby decreasing ROS generation and result in decreased allergic asthma. These data provide an understanding into p22phox dependent NADPH oxidase function(s) for the development of asthma.

Results

Asthmatic patients exhibit increased NADPH oxidase subunit p22phox

As p22phox is a vital subunit for the functional NADPH oxidase system to generate ROS, we investigated the expression of p22phox in human asthma samples by immunohistochemistry and real-time PCR. In healthy control biopsies positive immunoreactivity for p22phox was observed in the bronchial epithelium and lymphocytes. In biopsies from asthmatics more intense p22phox staining was observed in the bronchial epithelium and underlying smooth muscle layers (Figure 1A). The negative control for the immunohistochemistry is shown in Supplementary Figure 1). To quantify changes in p22phox expression, bronchial biopsy samples from healthy control and asthmatic patients were subjected to real-time PCR. In asthma patients the expression of p22phox was significantly increased in comparison to healthy samples (Figure 1B).

HDM treatment induces p22phox expression in mice

We next investigated the expression of p22phox in a murine model of experimental asthma (Supplementary Figure 2). In naïve mice expression of p22phox was predominately localised to bronchial epithelium and lung parenchymal cells (Figure 2A). Intranasal HDM treatment induced stronger p22phox immunoreactivity that was localised to areas of peribronchial inflammation, bronchial epithelium and airway smooth muscle cells (Figure 2A). Dual immunofluorescence revealed p22phox expression in both epithelial cells and in smooth muscle cells (Figure 2BC). To determine whether p22phox was also regulated in HDM treated mice we performed Western blotting. Increased p22phox levels were observed in HDM treated mice in comparison to controls (Figure 2D). All negative controls for immunostaining and western blotting are shown in Supplementary Figure 3. We also analysed the expression of NOX enzymes (NOX2, NOX4) and subunits (p40, p60, p67, NOXO1 and NOXA1) by real-time PCR (Supplementary Figure 4). Here we also observed a significant upregulation of the noxa1 activator subunit after HDM treatment.

HDM induced ROS production is dependent on p22phox

As p22phox is integral for ROS produced from NADPH oxidase, we investigated intracellular ROS production by measuring the superoxide levels in WT and mice defective in p22phox expression following treatment with PBS or HDM. Mice defective in p22phox ($Cyba^{nmf333}$) contain a point mutation within the p22phox gene which results in the absence of p22phox protein(35) and Supplementary Figure 3 and are here onwards called p22phox KO mice. In WT and KO PBS treated mice minimal levels of ROS were observed, while increased ROS levels was observed in WT mice treated with HDM (Figure 3). In contrast p22phox KO mice treated with HDM did not show any significant increased ROS production, demonstrating the importance of p22phox in generating HDM induced ROS production in the lung. The superoxide dismutase (SOD) quenchable signal is shown in Supplementary Figure 5. We next examined the expression of the anti-oxidative system in the WT and p22phox mice treated with HDM (Supplementary Figure 6). we observed a general trend for the decreased expression of catalase, SOD, Thioredoxin (THX), Glutathione Peroxidase (GPX) and peroxiredoxin (PRDX) isoforms, whereas PRDX6 was significantly lower expressed In HDM treated KO mice (Supplementary Figure 6).

p22phox knockout mice exhibit an altered inflammatory profile in response to HDM

We first confirmed HDM-sensitization in WT and KO mice, by measuring circulating HDM-specific immunoglobulins. HDM treatment showed an elevated IgG1a and IgG2c levels in the serum, were comparable between WT and KO mice. Furthermore HDM treatment significantly increased IgE levels only in WT mice, however in KO mice this increase did not reach significance (Supplementary Figure 7). To characterize the inflammatory profile the cellular composition of the BALF was analysed by flow cytometry. Treatment with HDM resulted in an increase in total cell counts in the BALF in both WT and KO mice (Figure 4A). Analysis of the cellular composition revealed higher numbers of eosinophils following HDM exposure in WT mice, this increase did not reach significance in KO mice. Elevated numbers of neutrophils, B cells, T cells and CD4+ and CD8+ T cell subsets were observed in

p22phox KO mice treatment with HDM compared to the WT counterparts. Analysis of the inflammatory cell recruitment by flow cytometry in lung homogenate samples revealed similar changes, with significantly increased eosinophils in WT mice and increased neutrophils in KO mice treated with HDM (Supplementary Figure 8). Analysis of cytokine levels in lung homogenate samples, revealed elevated IL4 and IL13 in WT mice treated with HDM, in HDM treated KO mice these changes were not significant (Figure 4B). In contrast IFNγ was only elevated in p22phox KO mice treated with HDM, this increase was absent in the WT mice treated for HDM (Figure 4B). We additionally profiled a number of cytokines by real-time PCR (Supplementary Figure 9). Both WT and KO mice possessed increased mRNA expression of the Th2 cytokines *IL-5* and *IL-13*. HDM treated KO mice possessed elevated levels of *IL-10* and *IL-17 mRNA*. The increased IL-17 was also accompanied by elevated *Cxcl1* (*Kc*) and *Cxcl2* (*Mip-2*) mRNA in KO mice treated with HDM in comparison to WT and control KO mice (Supplementary Figure 9).

p22phox knockout mice are protected from structural alterations in the airway epithelium

Due to the strong increase in p22phox levels in HDM treated mice, we next investigated whether deficiency in p22phox affects the development of goblet cell hyperplasia and mucus production following HDM treatment. Analysis and quantification of PAS stained lung sections revealed predominant goblet cell hyperplasia and mucus production in HDM treated wild-type mice. However, in p22phox KO mice, HDM treatment resulted in significantly reduced levels in comparison to HDM-treated WT mice (Figure 5). The PBS treated p22phox WT and KO mice did not show any changes in goblet cells and mucus production at basal levels.

Airway hyperreactivity is attenuated in p22phox-knockout mice

We next assessed an additional feature of asthma, airway hyperresponsiveness (AHR), as assessed by lung function measurements in response to increasing concentrations of inhaled methacholine (MCh). HDM treatment of WT mice resulted in an increased AHR at both 30 and 100 mg/ml MCh as demonstrated by increased airway resistance and elastance compared to PBS treated mice (Figure

6AB). Moreover, p22phox KO mice treated with HDM exhibited a significantly decreased AHR compared to HDM-treated WT mice (Figure 6AB). PBS treated p22phox WT and KO mice exhibited similar response to the increasing MCh concentrations.

p22phox-knockouts are less responsive to IL-13

As IL-13 is one of the key molecules controlling AHR(19), we investigated whether p22phox KO mice were protected from IL-13 induced AHR. To this end trachea ring segments were incubated overnight with IL-13, then a MCh dose response curve performed using a wire myograph. In the absence of IL-13 pre-incubation, both WT and KO tracheas produced a similar concentration-dependent increase in tracheal tension with increasing MCh concentrations. Pre-treatment of isolated WT tracheas with IL-13 strongly potentiated the response to increasing MCh doses. Similar to the in vivo AHR data, IL-13 incubation did not enhance AHR in KO mice (Figure 6C). In order to further understand the decreased IL-13 response, we analysed STAT6 activation in isolated tracheas with and without overnight IL-13 stimulation. In WT tracheas IL-13-induced a robust phosphorylation of STAT6, however, in KO tracheas the activation of STAT6 in response to IL-13 was not significantly increased (Figure 7AB). We also examined whether these results could be replicated by the use of ROS inhibitors. Pre-treatment with catalase but not N-acetyl-L-cysteine (NAC) was able to significantly inhibit the IL-13 induced phosphorylation of STAT6 (Figure 7C,D). Finally, we asked whether H_2O_2 stimulation was enough on its own to activate STAT6. As can be observed in Supplementary Figure 10, exogenous H_2O_2 alone was not sufficient to induce STAT6 phosphorylation.

Discussion

In this study we assessed the contribution of NADPH oxidase in the development of allergic asthma. The NADPH adaptor subunit p22phox (CYBA) was significantly upregulated in asthmatic patients and mice treated with HDM. Due to the essential role of p22phox in assembly and function of all major NOX isoforms (NOX1-4), loss of p22phox functional inactivates NADPH oxidase and consequently NADPH oxidase-derived ROS generation. Employing mice that lack the p22phox protein, we provide strong evidence that NADPH oxidase plays a crucial role in the HDM-induced development of AHR and goblet cell hyperplasia. We also show that IL-13-induced hypercontractility and signaling was significantly attenuated in bronchial rings from p22phox KO mice *ex vivo*. These protective effects could be attributed in part by the inability of p22phox KO mice to generate ROS (34). These findings support the notion that increased oxidative stress is integral in asthma pathogenesis and requires an active NADPH oxidase system

ROS derived from NADPH oxidase helps maintain vascular tone and can regulate important processes such as cytoskeletal organization, cell migration, growth, proliferation and apoptosis (18). In allergic animal models increased levels of oxidative stress and expression of antioxidant enzymes have been described (5,9). Accordingly, we here show that mice treated with HDM strongly induce the production of ROS. Elevated ROS species such as H_2O_2 have previously been measured in the exhaled breath condensate of asthma patients and correlates with disease severity (15,33). Due to this increased oxidative stress antioxidants such as peroxiredoxins, catalase and superoxide dismutase (SOD) maintain ROS levels in the lung and maintain the redox environment (20,21). In our study deficiency of p22phox was accompanied by loss of ROS production and associated with decreased goblet cell hyperplasia and AHR. Our results support the data of Sevin *et al.*, who analysed the OVA response in gp91phox (NOX2) KO mice and observed decreased goblet cell hyperplasia, AHR and eosinophilic inflammation (40). We expand on these observations, by demonstrating elevated expression of *p22-PHOX* in asthmatic bronchial biopsies and that p22phox essentially contributes to

mucus hypersecretion and AHR *in vivo* and *ex vivo*. Recently, Patel et al demonstrated that NADPH oxidases are required for mucin secretion in intestinal goblet cells (37). Increased NOX4 expression has been was reported in airway smooth muscle bundles and isolated smooth muscle cells of asthma patients. Furthermore, the hyper contractility phenotype of asthmatic SMC could be abrogated by anti-NOX4 siRNA or NOX inhibition (44). The presence of different SNPs in p22phox have been shown to associate with asthma, a homozygous 640A allele confers an increased risk while 640G a decreased risk (24). SNPs in the p22phox gene that result in lower expression or activity may reduce the prevalence of asthma while mutations that increase expression could promote asthma. It should also be considered that most of the patients presented in this study were being treated with ICS, about half of them on OCS.

One of the key Th2 cytokines involved in asthma pathogenesis is IL-13, neutralization of IL-13 signalling strongly attenuates allergen-induced AHR, mucus production and eosinophilia (19,49). Here we show that NADPH oxidase derived ROS is essential for the IL-13 driven AHR response. IL-13 can augment airway smooth muscle contractility via upregulation of RhoA and RhoA kinase (11,17), activated Rho kinase phosphorylates myosin light chain (MLC) and thereby enhances SMC contraction. Accordingly, application of the Rho-kinase inhibitor, Y-27632 leads to a significantly reduction in AHR (39,45). Our in vivo observations are further supported by the wire myograph experiments where direct incubation of tracheal rings with IL-13, failed to produce a hyper-response in p22phox KO mice. As we observed only strong induction of the IL-13 in HDM-treated WT mice, the protective effect observed in p22phox mice in AHR is most likely due to reduced IL-13 and IL-13 signalling within structural cells of the airways. This premise is supported by the decreased IL-13-induced activation of STAT6 in tracheal rings when p22phox is absent. Moreover pre-treatment with ROS inhibitors was able to diminish the IL-13 induced the activation of STAT6. Along these lines, it has been demonstrated that ROS inactivates the protein tyrosine phosphatase, PTP1B, which negatively regulates IL-4 receptor signalling via dephosphorylation of STAT6 (29,41). Therefore, loss

of p22phox and consequently NADPH dependent ROS production may promote dephosphorylation of pSTAT6 and thereby reduce IL-13 signalling.

The HDM induced increase in ROS levels could result from either recruited inflammatory cells or from the resident structural cells (e.g. epithelial or smooth muscle cells). One limitation of our study is that we could not differentiate between these two options as the presence of ROS was measured in the entire pulmonary lysate. Despite the protective effect on loss of p22phox has on AHR and goblet cell hyperplasia, KO mice possessed an altered inflammatory profile following HDM treatment. WT possessed high levels of the Th2 proteins IL-4 and IL-13, which was accompanied by strong eosinophil recruitment in the BALF and the lungs. On the other hand in KO mice these parameters were not significantly increased; instead elevated numbers of neutrophils and lymphocytes were observed. The elevated levels of IFNγ or *IL-17* in the HDM-treated KO mice could provide a mechanistic explanation for these observations. However, further experiments are required to decide between these two options. Earlier work by Snelgrove and colleagues has shown that a defect in $gp91^{phox}$ results in a skewed T cell response (43). T cell receptor ligation induces the production of hydrogen peroxide via the activation of NOX2. Hydrogen peroxide in turn activates the Th2 differentiation factors GATA-3 and STAT6 and inhibits the TH17 differentiation factor STAT3 (7,42,46). Therefore, loss of gp91phox or p22phox would alleviate the STAT3 inhibition and promote production of IL-17. Furthermore, IL-17 has been shown to increase the expression and stability of *Cxcl1* mRNA, thereby promoting neutrophil recruitment (13,28). These results are in line with our findings where the increased IL-17 expression observed in HDM-treated KO mice was associated with elevated *Cxcl1/2* mRNA expression and neutrophil recruitment. During the last decade, studies have underpinned the importance of ROS as a crucial secondary signalling messenger in many biological processes required for cellular homeostasis. The use of general ROS blockers like NAC might give conflicting results as it scavenges ROS regardless of their source (mitochondria/NADPH oxidase). A chronic increase in ROS levels should be tackled; however there is the caveat to not completely inhibit the basal ROS and affect the redox potential in the cell, which can alter cellular

homeostasis (47). Use of p22phox inhibitors might overcome these issues. Unfortunately, there are no commercially available p22phox inhibitors but by highlighting the importance of p22phox in asthma pathogenesis could further encourage their development.

In Conclusion these findings demonstrate the crucial role of p22phox dependent NADPH oxidase for the development of mucus hypersecretion and AHR in a mouse model of asthma. Elevated p22-PHOX expression in bronchial biopsies confirms the importance of the ROS generation from NADPH oxidase system in asthma pathogenesis.

Innovation

Increased ROS signalling and oxidative stress are strongly linked to the pathogenesis asthma, but to date there is little is known about NADPH oxidase role in development of asthmatic phenotype. We show for the first time increased p22phox expression in bronchial biopsies of asthmatic patients. We demonstrate oxidative stress/ROS from the p22phox-dependent NADPH oxidase is involved in signalling for AHR via activation of STAT6 in experimental induced asthma. Suggesting selective interference of p22phox might hold a promising therapeutic strategy for the management of asthma in clinical settings.

Materials and Methods

Human samples

Collection and use of bronchial biopsies from asthmatic patients and healthy control subjects was approved by the Southampton and South West Hampshire Joint Local Research Ethics Committee and written informed consent obtained from all study participants. Biopsies were obtained via bronchoscopy from healthy controls (n=16) and patients with asthma (n=35) this mixed cohort consists of 24% of Mild and remaining 76 % were severe asthmatic, some patients were included a previous study (30). Bronchial biopsies obtained were either immediately fixed in cold formalin and embedded in paraffin for further histological staining or immediately homogenised in Trizol Reagent and further processed for RNA isolation. The study Subjects' characteristics of healthy controls and asthmatic patients are summarized in Table 1

Animals and treatment protocol

p22phox KO mice ($Cyba^{nmf333}$) were obtained from Jackson Laboratories and bred in house. Mice were maintained under pathogen free conditions in isolated ventilated cages with 12 hour light/dark cycles. p22phox KO mice contain a T to C point mutation, which substitutes tyrosine for histidine at amino acid position 121 resulting in the inactivation and loss of the p22phox protein (35). Mice were maintained as a heterozygous colony; in order to reduce animal numbers, experimental mice were obtained by crossing homozygous parents to produce homozygous offspring. Water and chow were supplied ad libitum. All mouse experiments met EU guidelines 2010/63/EU and were approved by the Federal Ministry of Science, Research and Economics, Vienna, Austria. All measures were taken to keep animal suffering to a minimum. Mice were treated intra-nasally with a crude extract of HDM (50µg/25µl in phosphate buffered saline (PBS); Greer, Lenoir, NC, lot #187753) once per week for 6 weeks, while control mice received PBS. Analysis of lung function parameters and organ collection was performed 72 hours after the last challenge (Supplementary Figure 2).

Immunohistochemistry and immunofluorescence

Paraffin embedded bronchial biopsies and isolated perfused mouse lungs were cut into 3µm sections for histologic analysis. Sections were deparaffinized in xylene followed by decreasing concentrations of ethanol. Periodic acid–Schiff staining (PAS) was performed according to standard protocols. Immunostaining against p22phox (Human – Abcam (Cambridge, United Kingdom) 1:1000, Mouse - Santa Cruz (Heidelberg, Germany) 1:1000) was performed overnight using Sodium Citrate pH 6 treated sections. the specificity of the Immunohistochemistry and immunofluorescence staining was conformed with p22phox WT and KO lung tissue (Supplementary Figure 3) p22phox primary antibodies were detected by the immPRESS α-Rabbit Ig (peroxidase) polymer detection kit using NovaRed as the substrate (Vector Laboratories, Burlingame, CA); counterstaining was performed with Haemalaun (from Mayer). An Olympus VS120 slide scanning microscope was used to obtain images.

For double immunofluorescence the mouse lung sections were deparaffinised at 60°C overnight, and incubated in pH: 6 antigen retrieval solution at 95°C, followed by blocking with 10% BSA. Then samples were incubated overnight at 4°C with antibodies anti-p22phox (Abcam) along with anti-αSMA (#EB06450, Everest Biotech, Upper Heyford, UK) or pan-Cytokeratin (Biolegend, London, UK) in a concentration of 1:100 in 10% BSA, followed by incubation with Alexa Fluor -488, and -555 labelled secondary antibodies (Life Technologies, Carlsbad, CA, 1:500 in 0.1% BSA) for 45min at room temperature. Sections were counterstained with 4′,6-diamidino-2-phenylindole dihydrochloride (DAPI, Sigma-Aldrich, Dorset, UK) to visualize nuclei. Negative controls was performed alongside in each experiment were the primary antibody is omitted (Supplementary Figure 3). Images were taken using a laser scanning confocal microscope (Zeiss LMS 510 META; Zeiss, Jena, Germany) with Plan-Neofluar (40×/1.3 Oil DIC) objective. Brief details for p22phox staining, PAS were made according to standard protocols.

Quantitative histology

The percentage of goblet cells and mucus volume was quantified on PAS stained sections using the NewCast software (Visiopharm, Hoersholm, Denmark) on automatically selected randomly regions from the 20x scanned images. The Goblet and epithelial cells intersecting the airway basement membrane were counted and presented as percentage goblet cells; the volume of mucus was determined by point counts and compared to the surface area of the airway basement membrane as determined by line probe intersections (1,23).

Western blotting

Total proteins were isolated from lung homogenate or tracheal samples using RIPA buffer (Sigma) and separated on a SDS-PAGE polyacrylamide gel and transferred to a PVDF membrane (GE Healthcare, Vienna, Austria). After blocking with 5% non-fat dry milk in TBS-Tween (0.1%) buffer, the membrane was incubated overnight at 4 °C with the following antibodies: anti-p22phox (Santa Cruz 1:100), p-STAT6 (1:1000) or anti-α-tubulin (1:4000; all from Cell Signaling, Danvers, MA). Horse radish peroxidase-conjugated goat anti-rabbit secondary antibodies together with the ECL prime (GE Healthcare) developing solution was used to detect primary antibodies. Equal protein loading and transfer was controlled by normalising to α-tubulin. The p22phox protein size was conformed the western blot with p22phox WT and KO lung tissue (Supplementary figure 3). Uncropped western blots are given in the supplementary data (Supplementary figure 11).

Intracellular reactive oxygen species (ROS) measurements

The levels of hydrogen peroxide or superoxide were determined by changes in intracellular H2DCF-DA or DHE (Life Technologies, Vienna, Austria) fluorescence levels respectively. Briefly, single cell lung tissue homogenates were prepared by digesting the lower right lube with Collagenase (200ng/ml) and DNAse (200ng/ml) for 40 min at 37°C. The tissue homogenate was passed through cell strainer (100µm) for single cell suspension and if necessary erythrocytes were lysed with erythrolysis buffer (2.6mM NH4Cl, 0.09M KCO3, 0.6M Titriplex III). Cells (100,000) were loaded with

H2DCF-DA (10µM) or DHE (10µM) for 45 min at 37°C. Fluorescence activation of H2DCF-DA was measured at 504-nm excitation and 529-nm emission, for DHE the measurement were observed at 535 nm excitation and 635 nm emission. Blank (cell fraction without H2DCF-DA or DHE) readings were subtracted from loaded sample readings. SOD quenchable signal were also measured in PBS and HDM treated lung homogenate, the SOD inhibited the HDM induced increase in ROS both in H2DCFDA or DHE fluorescent levels (Supplementary figure 5)

Cytokines and Immunoglobulin detection

Blood was collected from the vena cava and serum levels of HDM specific immunoglobulin (Ig)E, IgG1a and IgG2c were measured by ELISA. In summary 96 well plates (Maxisorb, Greiner, Kremsmünster, Austria) were coated overnight with HDM at a concentration of 200µg/ml, 5µg/ml or 50µg/ml for IgE, IgG1 or IgG2, respectively, in coating buffer containing 0.84% $NaHCO_3$ in H_2O (pH 8.3). Serum samples were diluted in PBS containing 0.1% Tween and incubated overnight. Specific immunoglobulin subtypes were identified using a biotinylated anti-IgE, IgG1 or IgG2 antibodies (BD Biosciences, Heidelberg, Germany). Following incubation with streptavidin conjugated with horse radish peroxidase, the chromogenic substrate BM Blue POD Substrate (Roche, Mannheim, Germany) was used for development. For quantitative measurement of mouse IL-4, IL-13 and IFNγ (eBioscience, Vienna, Austria), in mice lung homogenate, ELISAs were performed according to the manufacturer's instructions.

Bronchoalveolar lavage fluid (BALF)

After animals were sacrificed, BALF was obtained using 1 ml PBS containing protease inhibitor cocktail (Roche).

Flow cytometry

BAL and single cell lung tissue homogenates were analysed using a LSRII flow cytometer and analysed with the FACSDiva software (BD Biosciences). Cells were identified as follows: neutrophils

(CD11b+, CD11c-, Gr-1+), macrophages (CD11b low, CD11c+, Siglec F+), dendritic cells (CD11b+, CD11c+, MHC-II high), T helper cells (CD3+, CD4+), cytotoxic T cells (CD3+, CD8+), B cells (CD19+), and eosinophils cells (CD11b+, CD11c-, Siglec F+). Antibody details are provided in the Table 2.

RNA isolation and real time PCR analysis

Real time analysis of p22-PHOX (CYBA) expression in human samples used the Taqman probe Hs03044361_m1 (Life Technologies, UK), Glyceraldehyde 3-phosphate dehydrogenase (GADPH) was used as the reference gene (PrimerDesign, Southampton, UK. Data is presented as ΔΔCt. For the analysis of mouse samples total RNA was isolated from lung homogenate samples using a peqGOLD Total RNA Kit (Peqlab, Erlangen, Germany). cDNA synthesis and real-time PCR was performed as described previously (20). Briefly, total RNA was reverse transcribed using the iScript™ cDNA Synthesis kit (Bio-Rad Laboratories, Hercules, CA, USA), according to manufacturer's instructions. Real-time PCR was performed using a LightCycler® 480 System (Roche Applied Science, Wien, Austria). The PCR reactions were set up using a QuantiFast® SYBR® Green PCR kit (Qiagen, Hilden, Germany) using the following protocol 5 min at 95°C, (5 sec at 95°C, 5 sec at 60°C, and 10 sec at 72°C) ×45. Due to the nonselective double-strand DNA binding of the SYBR® Green I dye, melting curve analysis and gel electrophoresis were performed to confirm the specific amplification of the expected PCR products. Pbgd and B2m were used as the reference genes. The difference in threshold cycle (Ct) values for each target gene was calculated as follows: ΔCt = meanCt reference genes – Ct target gene. Primer sequences are given Table 3.

Assessment of airway hyperactivity

Seventy two hours after the final HDM or PBS challenge, mice were anesthetized, intubated, and mechanically ventilated for the measurements of airway resistance and elastance (reciprocal of compliance) using a FlexiVent (SciReq, Inc., Montreal, PQ, Canada). Changes in airway resistance and elastance were calculated as response to increasing concentrations of methacholine (0, 1, 3, 10, 30 and 100 mg/ml, Sigma Aldrich) as previously described (26). Briefly, mice were deeply anesthetised

with 150 mg/kg ketamine, 20mg/kg xylazine and were ventilated at 150 breaths/min, tidal volume of 10 ml/kg and a positive end expiratory pressure of 2cmH2O. Each data point represents the average of twelve snapshot perturbations recorded over a three minute period after each methacholine dose; before each set of perturbations two deep inflation manoeuvres were performed to normalise lung volume.

Tracheal stimulation and Wire myograph

For Tracheal stimulation, the samples were cleaned of surrounding adipose and connective tissue is incubated with or without IL-13 (50 ng/ml) in the presence and absence of n-acetyl cysteine [NAC] (1 µM), catalase (10 u/ml) and H_2O_2 (200 µM) for an hour and the tissue samples are snap frozen in liquid nitrogen and stored in-80°C until protein isolation.For isometric tension measurements, tracheal samples were cleaned of surrounding adipose and connective tissue and cut into segments ~2 mm in length for use in isometric tension measurements. The tracheal tissues were incubated with or without murine IL-13 (Ebioscience, Vienna, Austria) overnight in DMEM supplemented with 10mM HEPES and antibiotics. Tracheas were positioned between two adjustable pins in a myograph chamber (Multi Wire Myograph System-620M; Danish MyoTechnology A/S, Aarhus, Denmark) containing physiologic salt solution and continuously aerated with 95% O2, 5% CO2 at 37°C. The myograph chambers were connected to force transducers for isometric tension measurements (PowerLab® 8/35; ADInstruments, Dunedin, New Zealand)(25) .Tracheas were incubated at 37°C, and a basal tension of 2 mN was applied and allowed to stabilise for 45 min. Physiologic salt solution containing 120 mM KCl was used to determine viability and adequate contractility of the tissues. Tracheas were stimulated three times, using 120 mM KCl to obtain reproducible contractions. Tracheas that did not respond to these repeated stimuli were not included in the study. Methacholine was introduced in 4 min intervals in accumulative doses.

Statistical analysis

Statistical analysis was performed using GraphPad Prism 5/6 software. Data are expressed as mean ± SEM or box-and-whiskers plots. For normally distributed data inter group variants were compared by Student's t-tests, otherwise by Mann-Whitney U test. Multi-group comparisons were made with One-way ANOVA with Tukey’s post-hoc test. For comparison of dose-response curves or progressive measurements between groups two-way ANOVA was used with Bonferroni’s post-hoc test. P values <0.05 were considered as statistically significant.

Acknowledgements

Excellent technical assistance from Sabrina Reinisch, Camilla Götz, Thomas Fuchs, Eva Grasmann and Sabine Halsegger are appreciated. We would like to thank Grazyna Kwapiszewska for fruitful discussions. Leigh Marsh and Hans Michael Haitchi are members of COST (Cooperation in Science and Technology) Action BM1201. HMH was supported by a Medical Research Council (MRC) Clinician Scientist Fellowship (G0802804) and human samples were studied from the Wessex severe asthma cohort, which was supported by a MRC grant (G0800649) to PHH. Akos Heinemann received grant support from the Austrian Science Funds FWF (P22521-B18).

Author Disclosure Statement

The authors declare that there are no relevant conflicts of interests.

List of abbreviations:

AHR- Airway hyperresponsiveness;

BALF- Bronchoalveolar lavage fluid;

BDP -beclomethasone dipropionate ;

DHE- Dihydroethidium;

HDM-House Dust Mite;

H2DCFDA- 2',7'-dichlorodihydrofluorescein diacetate;

ICS -inhaled corticosteroids;

KO-p22phox Knockout mouse;

WT-p22phox Wild-type littermate mouse

OCS- oral corticosteroids;

PBS-Phosphate buffered saline;

PSS-physiological salt solution:

ROS-Reactive oxygen species;

SABA - short-acting ßeta2-agonists;

References

1. Alrifai M, Marsh LM, Dicke T, Kilic A, Conrad ML, Renz H and Garn H. Compartmental and temporal dynamics of chronic inflammation and airway remodelling in a chronic asthma mouse model. *PLoS One* 9: e85839, 2014.

2. Ambasta RK, Kumar P, Griendling KK, Schmidt HH, Busse R and Brandes RP. Direct interaction of the novel Nox proteins with p22phox is required for the formation of a functionally active NADPH oxidase. *J Biol Chem* 279: 45935-45941, 2004.

3. Banerjee ER and Henderson WR,Jr. Role of T cells in a gp91phox knockout murine model of acute allergic asthma. *Allergy Asthma Clin Immunol* 9: 6-1492-9-6, 2013.

4. Banerjee ER and Henderson WR,Jr. Defining the molecular role of gp91phox in the immune manifestation of acute allergic asthma using a preclinical murine model. *Clin Mol Allergy* 10: 2-7961-10-2, 2012.

5. Barnes PJ. Reactive oxygen species and airway inflammation. *Free Radic Biol Med* 9: 235-243, 1990.

6. Bedard K and Krause KH. The NOX family of ROS-generating NADPH oxidases: physiology and pathophysiology. *Physiol Rev* 87: 245-313, 2007.

7. Belikov AV, Schraven B and Simeoni L. T cells and reactive oxygen species. *J Biomed Sci* 22: 85-015-0194-3, 2015.

8. Bousquet J, Jeffery PK, Busse WW, Johnson M and Vignola AM. Asthma. From bronchoconstriction to airways inflammation and remodeling. *Am J Respir Crit Care Med* 161: 1720-1745, 2000.

9. Bowler RP and Crapo JD. Oxidative stress in allergic respiratory diseases. *J Allergy Clin Immunol* 110: 349-356, 2002.

10. Brightling CE, Symon FA, Birring SS, Bradding P, Pavord ID and Wardlaw AJ. TH2 cytokine expression in bronchoalveolar lavage fluid T lymphocytes and bronchial submucosa is a feature of asthma and eosinophilic bronchitis. *J Allergy Clin Immunol* 110: 899-905, 2002.

11. Chiba Y, Nakazawa S, Todoroki M, Shinozaki K, Sakai H and Misawa M. Interleukin-13 augments bronchial smooth muscle contractility with an up-regulation of RhoA protein. *Am J Respir Cell Mol Biol* 40: 159-167, 2009.

12. Cockcroft DW and Davis BE. Mechanisms of airway hyperresponsiveness. *J Allergy Clin Immunol* 118: 551-9; quiz 560-1, 2006.

13. Datta S, Novotny M, Pavicic PG,Jr, Zhao C, Herjan T, Hartupee J and Hamilton T. IL-17 regulates CXCL1 mRNA stability via an AUUUA/tristetraprolin-independent sequence. *J Immunol* 184: 1484-1491, 2010.

14. Dworski R. Oxidant stress in asthma. *Thorax* 55 Suppl 2: S51-3, 2000.

15. Emelyanov A, Fedoseev G, Abulimity A, Rudinski K, Fedoulov A, Karabanov A and Barnes PJ. Elevated concentrations of exhaled hydrogen peroxide in asthmatic patients. *Chest* 120: 1136-1139, 2001.

16. Frazziano G, Champion HC and Pagano PJ. NADPH oxidase-derived ROS and the regulation of pulmonary vessel tone. *Am J Physiol Heart Circ Physiol* 302: H2166-77, 2012.

17. Goto K, Chiba Y, Matsusue K, Hattori Y, Maitani Y, Sakai H, Kimura S and Misawa M. The proximal STAT6 and NF-kappaB sites are responsible for IL-13- and TNF-alpha-induced RhoA transcriptions in human bronchial smooth muscle cells. *Pharmacol Res* 61: 466-472, 2010.

18. Griendling KK and Ushio-Fukai M. Reactive oxygen species as mediators of angiotensin II signaling. *Regul Pept* 91: 21-27, 2000.

19. Grunig G, Warnock M, Wakil AE, Venkayya R, Brombacher F, Rennick DM, Sheppard D, Mohrs M, Donaldson DD, Locksley RM and Corry DB. Requirement for IL-13 independently of IL-4 in experimental asthma. *Science* 282: 2261-2263, 1998.

20. Hanschmann EM, Godoy JR, Berndt C, Hudemann C and Lillig CH. Thioredoxins, glutaredoxins, and peroxiredoxins--molecular mechanisms and health significance: from cofactors to antioxidants to redox signaling. *Antioxid Redox Signal* 19: 1539-1605, 2013.

21. Hoffmann J, Wilhelm J, Marsh LM, Ghanim B, Klepetko W, Kovacs G, Olschewski H, Olschewski A and Kwapiszewska G. Distinct differences in gene expression patterns in pulmonary arteries of patients with chronic obstructive pulmonary disease and idiopathic pulmonary fibrosis with pulmonary hypertension. *Am J Respir Crit Care Med* 190: 98-111, 2014.

22. Hoffmann J, Wilhelm J, Marsh LM, Ghanim B, Klepetko W, Kovacs G, Olschewski H, Olschewski A and Kwapiszewska G. Distinct differences in gene expression patterns in pulmonary arteries of patients with chronic obstructive pulmonary disease and idiopathic pulmonary fibrosis with pulmonary hypertension. *Am J Respir Crit Care Med* 190: 98-111, 2014.

23. Hsia CC, Hyde DM, Ochs M, Weibel ER and ATS/ERS Joint Task Force on Quantitative Assessment of Lung Structure. An official research policy statement of the American Thoracic Society/European Respiratory Society: standards for quantitative assessment of lung structure. *Am J Respir Crit Care Med* 181: 394-418, 2010.

24. Izakovicova Holla L, Kankova K and Znojil V. Haplotype analysis of the NADPH oxidase p22 phox gene in patients with bronchial asthma. *Int Arch Allergy Immunol* 148: 73-80, 2009.

25. Jain PP, Leber R, Nagaraj C, Leitinger G, Lehofer B, Olschewski H, Olschewski A, Prassl R and Marsh LM. Liposomal nanoparticles encapsulating iloprost exhibit enhanced vasodilation in pulmonary arteries. *Int J Nanomedicine* 9: 3249-3261, 2014.

26. Konya V, Maric J, Jandl K, Luschnig P, Aringer I, Lanz I, Platzer W, Theiler A, Barnthaler T, Frei R, Marsche G, Marsh LM, Olschewski A, Lippe IT, Heinemann A and Schuligoi R. Activation of EP4 receptors prevents endotoxin-induced neutrophil infiltration into the airways and enhances microvascular barrier function. *Br J Pharmacol*, 2015.

27. Kwon BI, Kim TW, Shin K, Kim YH, Yuk CM, Yuk JM, Shin DM, Jo EK, Lee CH and Lee SH. Enhanced Th2 cell differentiation and function in the absence of Nox2. *Allergy* 72: 252-265, 2017.

28. Laan M, Cui ZH, Hoshino H, Lotvall J, Sjostrand M, Gruenert DC, Skoogh BE and Linden A. Neutrophil recruitment by human IL-17 via C-X-C chemokine release in the airways. *J Immunol* 162: 2347-2352, 1999.

29. Lu X, Malumbres R, Shields B, Jiang X, Sarosiek KA, Natkunam Y, Tiganis T and Lossos IS. PTP1B is a negative regulator of interleukin 4-induced STAT6 signaling. *Blood* 112: 4098-4108, 2008.

30. Maeda Y, Chen G, Xu Y, Haitchi HM, Du L, Keiser AR, Howarth PH, Davies DE, Holgate ST and Whitsett JA. Airway epithelial transcription factor NK2 homeobox 1 inhibits mucous cell metaplasia and Th2 inflammation. *Am J Respir Crit Care Med* 184: 421-429, 2011.

31. Montuschi P BP. **Isoprostanes and asthma**. *3* 3: 287-292, 2006.

32. Montuschi P and Barnes PJ. New perspectives in pharmacological treatment of mild persistent asthma. *Drug Discov Today* 16: 1084-1091, 2011.

33. Montuschi P, Barnes PJ and Ciabattoni G. Measurement of 8-isoprostane in exhaled breath condensate. *Methods Mol Biol* 594: 73-84, 2010.

34. Nakano Y, Longo-Guess CM, Bergstrom DE, Nauseef WM, Jones SM and Banfi B. Mutation of the Cyba gene encoding p22phox causes vestibular and immune defects in mice. *J Clin Invest* 118: 1176-1185, 2008.

35. Nakano Y, Longo-Guess CM, Bergstrom DE, Nauseef WM, Jones SM and Banfi B. Mutation of the Cyba gene encoding p22phox causes vestibular and immune defects in mice. *J Clin Invest* 118: 1176-1185, 2008.

36. Panina-Bordignon P, Papi A, Mariani M, Di Lucia P, Casoni G, Bellettato C, Buonsanti C, Miotto D, Mapp C, Villa A, Arrigoni G, Fabbri LM and Sinigaglia F. The C-C chemokine receptors CCR4 and CCR8 identify airway T cells of allergen-challenged atopic asthmatics. *J Clin Invest* 107: 1357-1364, 2001.

37. Patel KK, Miyoshi H, Beatty WL, Head RD, Malvin NP, Cadwell K, Guan JL, Saitoh T, Akira S, Seglen PO, Dinauer MC, Virgin HW and Stappenbeck TS. Autophagy proteins control goblet cell function by potentiating reactive oxygen species production. *EMBO J* 32: 3130-3144, 2013.

38. Pendyala S, Usatyuk PV, Gorshkova IA, Garcia JG and Natarajan V. Regulation of NADPH oxidase in vascular endothelium: the role of phospholipases, protein kinases, and cytoskeletal proteins. *Antioxid Redox Signal* 11: 841-860, 2009.

39. Schaafsma D, Bos IS, Zuidhof AB, Zaagsma J and Meurs H. Inhalation of the Rho-kinase inhibitor Y-27632 reverses allergen-induced airway hyperresponsiveness after the early and late asthmatic reaction. *Respir Res* 7: 121, 2006.

40. Sevin CM, Newcomb DC, Toki S, Han W, Sherrill TP, Boswell MG, Zhu Z, Collins RD, Boyd KL, Goleniewska K, Huckabee MM, Blackwell TS and Peebles RS,Jr. Deficiency of gp91phox inhibits allergic airway inflammation. *Am J Respir Cell Mol Biol* 49: 396-402, 2013.

41. Sharma P, Chakraborty R, Wang L, Min B, Tremblay ML, Kawahara T, Lambeth JD and Haque SJ. Redox regulation of interleukin-4 signaling. *Immunity* 29: 551-564, 2008.

42. Shatynski KE, Chen H, Kwon J and Williams MS. Decreased STAT5 phosphorylation and GATA-3 expression in NOX2-deficient T cells: role in T helper development. *Eur J Immunol* 42: 3202-3211, 2012.

43. Snelgrove RJ, Edwards L, Williams AE, Rae AJ and Hussell T. In the absence of reactive oxygen species, T cells default to a Th1 phenotype and mediate protection against pulmonary Cryptococcus neoformans infection. *J Immunol* 177: 5509-5516, 2006.

44. Sutcliffe A, Hollins F, Gomez E, Saunders R, Doe C, Cooke M, Challiss RA and Brightling CE. Increased nicotinamide adenine dinucleotide phosphate oxidase 4 expression mediates intrinsic airway smooth muscle hypercontractility in asthma. *Am J Respir Crit Care Med* 185: 267-274, 2012.

45. Taki F, Kume H, Kobayashi T, Ohta H, Aratake H and Shimokata K. Effects of Rho-kinase inactivation on eosinophilia and hyper-reactivity in murine airways by allergen challenges. *Clin Exp Allergy* 37: 599-607, 2007.

46. Tse HM, Thayer TC, Steele C, Cuda CM, Morel L, Piganelli JD and Mathews CE. NADPH oxidase deficiency regulates Th lineage commitment and modulates autoimmunity. *J Immunol* 185: 5247-5258, 2010.

47. Ursini F, Maiorino M and Forman HJ. Redox homeostasis: The Golden Mean of healthy living. *Redox Biol* 8: 205-215, 2016.

48. van der Vliet A. Nox enzymes in allergic airway inflammation. *Biochim Biophys Acta* 1810: 1035-1044, 2011.

49. Wills-Karp M, Luyimbazi J, Xu X, Schofield B, Neben TY, Karp CL and Donaldson DD. Interleukin-13: central mediator of allergic asthma. *Science* 282: 2258-2261, 1998.

Table 1: Subject characteristics of bronchial biopsies group

	Healthy Control (n=16)	Asthma (n=35)
Age, yr	26 (18-55)	43 (18-69)*
Sex m/f	9/7	11/24
Atopy	5	21
FEV_1% predicted	97 (83-141)	82 (20-113)#
BTS Step	0	1-5
SABA	N/A	35
ICS	N/A	30
LABA	N/A	29
OCS	N/A	14

In accordance with the British guideline on the management of asthma (British Thoracic Society & Scottish Intercollegiate Guidelines Network) Thorax 2014;69: Suppl 1 i1-i192, Step1: Inhaled short-acting ß2-agonists (SABA) as required. Step2: SABA + inhaled corticosteroids [ICS] 200-800 µg beclomethasone dipropionate [BDP] or equivalent/day. Step3: SABA + ICS + inhaled long-acting ß2-agonists [LABA]. Step 4: Up to 2000 µg/day ICS + LABA + others. Step 5: Up to 2000 µg/day ICS + oral steroids (OCS). * Mann Whitney U test; #Student t-test ($p<0.05$)

Table 2: BAL and single cell lung tissue homogenates were analysed by flow cytometer with the following antibodies. Cells were identified as follows: neutrophils (CD11b+, CD11c-, Gr-1+), macrophages (CD11b low, CD11c+, siglec-F+), dendritic cells (CD11b+, CD11c+, MHC-II high), T helper cells (CD3+, CD4+), cytotoxic T cells (CD3+, CD8+), B cells (CD19+), and eosinophils cells (CD11b+, CD11c-, Siglec F+).

Antigen	Label	Company	Clone	Isotype	Dilution
CD3	FITC	eBioscience	145-2C11	Hamster IgG	20
CD4	APC	Biolegend	GK1.5	Rat IgG2b, κ	100
CD8	PE	Biolegend	53-6.7	Rat IgG2a, κ	200
CD11b	V500	BD Bioscience	M1/70	Rat IgG2b, κ	50
CD11c	ef450	eBioscience	N418	Armenian Hamster IgG	50
CD19	AF700	Biolegend	6D5	Rat IgG2a, κ	100
CD24	PerCP Cy5.5	BD Bioscience	M1/69	Rat IgG2b, κ	500
CD25	APC-Cy7	Biolegend	PC61	Rat IgG1, λ	50
CD45	PerCP-Cy5.5	eBioscience	30-F11	Rat IgG2b, κ	200
CD45	FITC	Biolegend	30-F11	Rat IgG2b, κ	200
CD64	AF647	BD Bioscience	X54-5/7.1	Mouse NOD/Lt IgG1, κ	20
gdTCR	BV421	Biolegend	GL3	Hamster IgG	50
Gr-1	PE-Cy7	Biolegend	RB6-8C5	Rat IgG2b, κ	800
MHC-II	APC-Cy7	Biolegend	M5/114.15.2	Rat IgG2b, κ	400
Siglec F	PE	BD Bioscience	E50-2440	Rat IgG2a, κ	20

Table 3: Primer sequences for real-time PCR

Gene	Species	Accession No.	Forward primer (5'-3')	Forward primer (3'-5')	Amplicon (bp)
CYBA	*Hu*	NM_000101.3	Taqman probe		-
GAPDH	*Hu*	NM_001256799	Taqman probe		-
UBC	*Hu*	NM_021009.6	Taqman probe		-
IL-5	*Mu*	NM_010558.1	AAG CAA TGA GAC GAT GAG GCT	CCC CAC GGA CAG TTT GAT TCT	110
IL-10	*Mu*	NM_010548.2	AGG CGC TGT CAT CGA TTT CT	ATG GCC TTG TAG ACA CCT TGG	104
IL-13	*Mu*	NM_008355.3	GCC AAG ATC TGT GTC TCT CCC	CCA GGT CCA CAC TCC ATA CC	115
IL-17A	*Mu*	NM_010552.3	AGG ACG CGC AAA CAT GAG TC	GGA CAC GCT GAG CTT TGA GG	119
IFNγ	*Mu*	NM_008337.3	CAG CAA CAG CAA GGC GAA AAA GG	TTT CCG CTT CCT GAG GCT GGA T	145
B2M	*Mu*	NM_009735.3	CGG CCT GTA TGC TAT CCA GAA AAC C	TGT GAG GCG GGT GGA ACT GTG	115
PBGD	*Mu*	NM_001110251	GCC AGA GAA AAGT GCC GTG GG	TCC GGA GGC GGG TGT TGA GG	115

Figure legends

Figure 1. Increased p22-PHOX (CYBA) expression in bronchial biopsies from asthmatic patients

A) Localisation of p22-PHOX by immunohistochemical staining in bronchial biopies of healthy and asthma patient. Brown indicates positive staining, nuclei are counterstained with Haemalaun (purple); + indicates smooth muscle cells, * epithelium and ^{o} inflammatory cells, scale bar represents 50 µm. Relative expression of *p22-PHOX* mRNA in B) bronchial biopsies derived from healthy individuals and patients with asthma. Lines represent median *p≤ 0.05.

Figure 2. Enhanced p22phox expression in mice lung treated with HDM

A) Representative immunohistochemical staining against p22phox in lungs of PBS and HDM treated wild-type mice, positive p22phox staining (brown), with nuclei counterstaining with methyl green. scale bar represents 100µm. B) Representative co-immunofluorescent staining to visualizing p22phox (red) co-stained with cytokeratin (green) for epithelial cells and C) αSMA (green) for the smooth muscle cells from the lungs of PBS and HDM treated wild-type mice. Scale bars indicate 20µm. D) Levels of p22phox protein expression in lung homogenates of wild-type mice treated with PBS and HDM, equal protein loading was confirmed by α tubulin (α-Tub), corresponding densitometric analysis is shown in the right panel (n = 4), data are presented as mean ± SEM, *p≤ 0.05.

Figure 3. HDM induced ROS production is diminished in p22phox KO mice

Changes in ROS production in single cell lung preparation from WT and KO mice treated with or without HDM as detected by A) H_2DCFDA and B) DHE fluorescence for detection of superoxides, respectively. Tukey box plots show medians, n = 4-5, *p ≤ 0.05, **p ≤ 0.01.

Figure 4. Inflammatory cell recruitment and cytokine profiling in p22phox KO and WT mice treated with HDM

A) Flow cytometric analysis of the BALF from mice treated with PBS or HDM, data is expressed as total cell numbers. B) Expression analysis of inflammatory cytokines in lung homogenate samples of p22phox KO and WT mice treated with PBS or HDM by ELISA. Tukey boxplots show medians, n = 4-8, $^{**}p \leq 0.01$, $^{***}p \leq 0.001$.

Figure 5. Reduced mucus and goblet cell hyperplasia in p22phox mice after intranasal HDM challenge

A) Representative images of Periodic acid-Schiff stained slides to detect mucus producing goblet cells in the airways from lungs of p22phox WT and p22phox KO mice treated with PBS or HDM, scale bar indicates 100 µm. Quantification of PAS staining, B) percentage of goblet cells and (C) mucus volume. Tukey boxplot show medians, n = 6-8, $^{***}p \leq 0.001$. (To see this illustration in color the reader is referred to the web version of this article at www.liebertonline.com/ars)

Figure 6. p22phox-KO mice are protected from to HDM and IL-13 induced airway hyperreactivity

Invasive lung function test to measure changes in A) airway resistance (R) and B) elastance (E) in response to increasing doses of methacholine (MCh) in WT and p22phox KO mice treated with PBS or HDM. C) Isometric tension experiments using tracheal rings treated with and without overnight incubation with IL-13 in p22phox WT and p22phox KO mice with increasing concentration of MCh, gram (g). Data are presented as mean ± SEM, values were analyzed with two-way ANOVA with Bonferroni post-hoc test. n = 4-6,$^{*}p \leq 0.05$, $^{**}p \leq 0.01$, $^{***}p \leq 0.001$ vs PBS treated mice; $^{\#}p \leq 0.05$, $^{\#\#}p \leq 0.01$, $^{\#\#\#}p \leq 0.001$ vs HDM treated mice.

Figure 7. Decreased STAT6 activation following IL-13 stimulation in p22phox-KO mice

A) Levels of STAT6 phosphorylation in tracheal rings isolated from p22phox WT and p22phox KO mice and treated with and without IL-13 (100 ng/ml). Equal protein loading was confirmed by α

tubulin (α-Tub). B) Corresponding densitometric analysis is shown (n=3-4),*p ≤ 0.01. C) IL-13 induced phospho STAT6 levels in the presence and absence of antioxidant N-acetyl-L-cysteine (NAC) and catalase. D) Corresponding densitometric analysis is shown (n=8-10) **p ≤ 0.01, ***p ≤ 0.001

Figure 1.

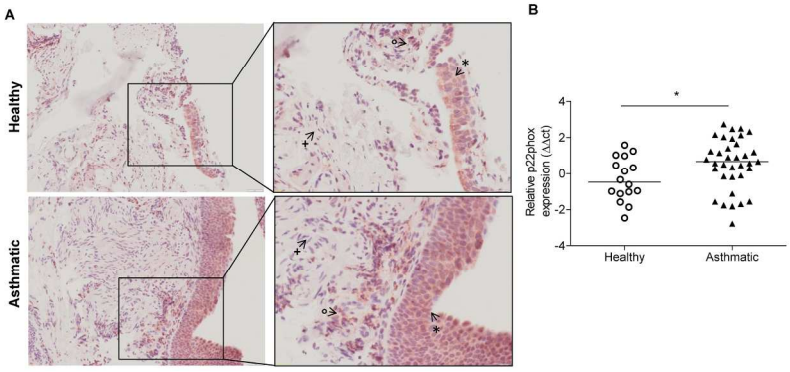

figure 1

209x148mm (300 x 300 DPI)

Figure 2.

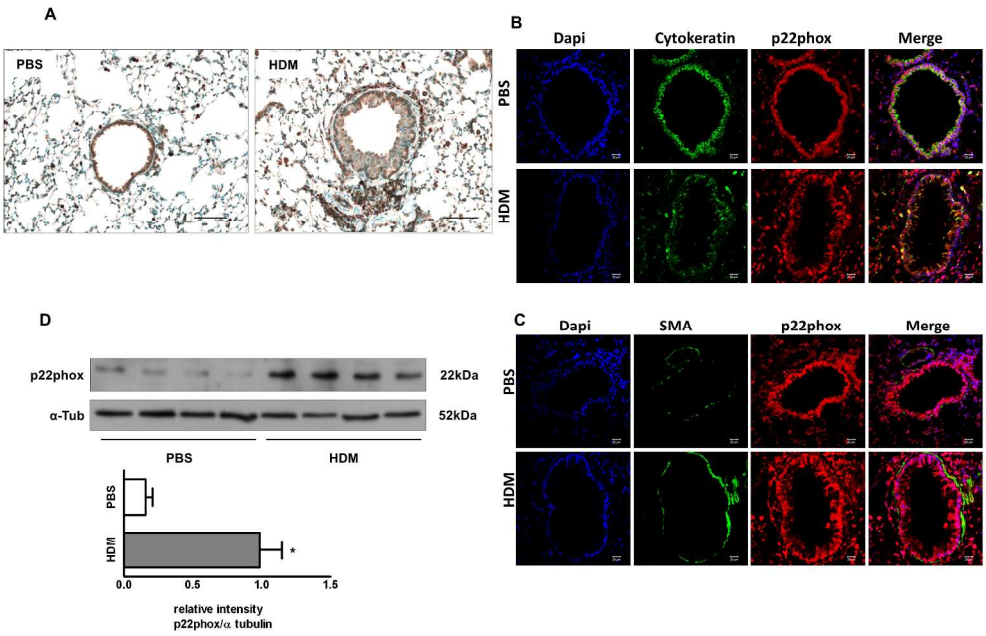

figure 2

762x571mm (96 x 96 DPI)

Figure 3.

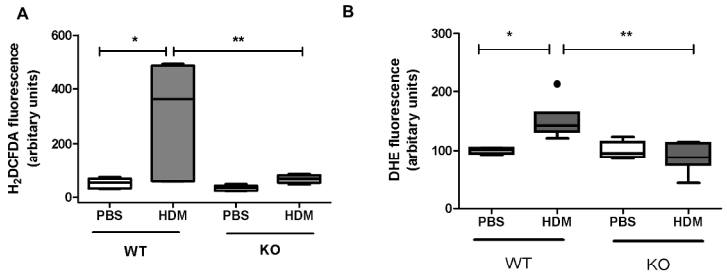

figure 3

762x571mm (96 x 96 DPI)

Figure 4.

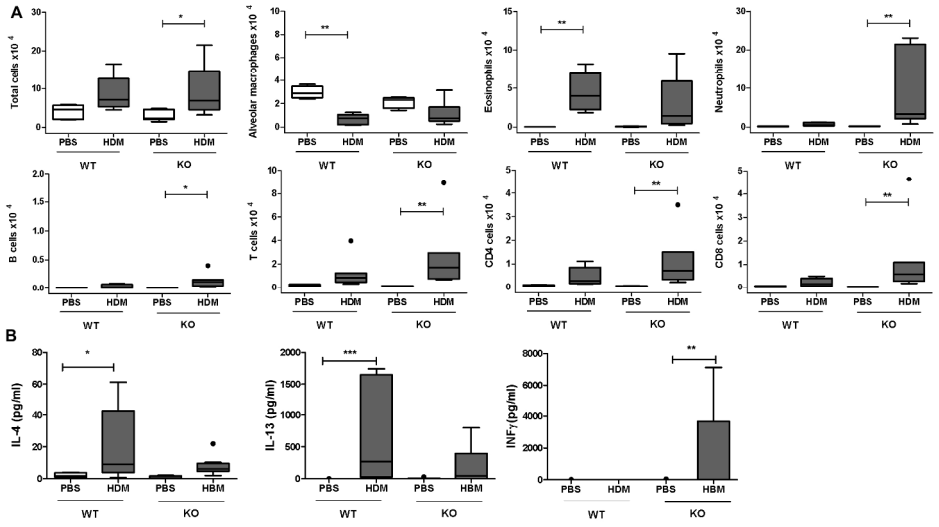

figure 4

762x571mm (96 x 96 DPI)

Figure 5.

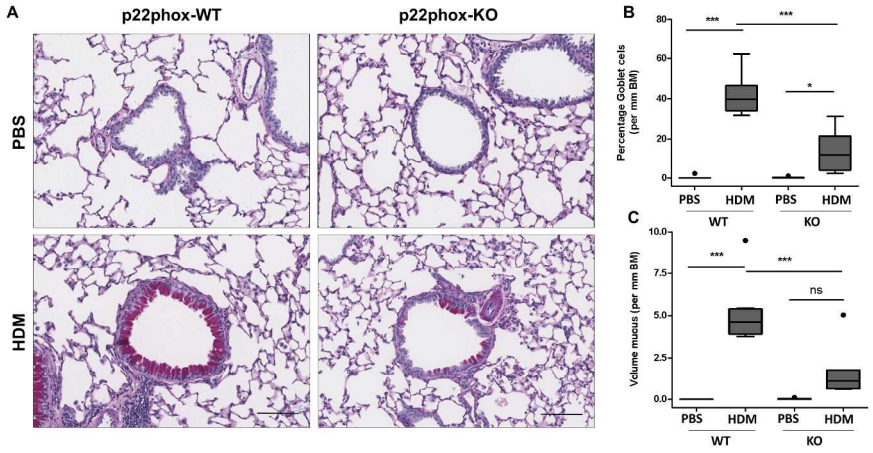

figure 5

762x571mm (96 x 96 DPI)

Figure 6.

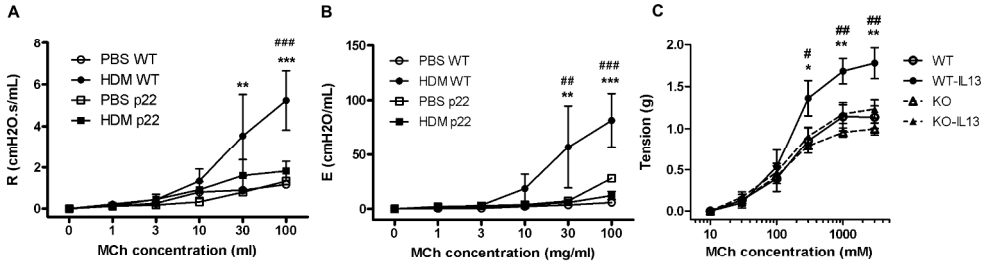

figure 6

762x571mm (96 x 96 DPI)

Figure 7.

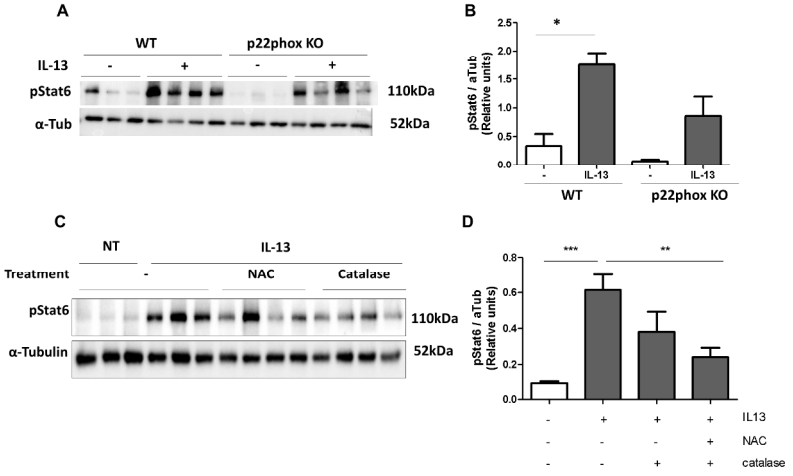

figure 7

762x571mm (96 x 96 DPI)

Online Repository

Increased expression of p22phox mediates airway hyperresponsiveness in an experimental model of asthma

Chandran Nagaraj PhD[1], Hans Michael Haitchi MD, PhD[2,3,4], Akos Heinemann MD[5], Peter H. Howarth MD, DM[3], Andrea Olschewski MD[1,6], Leigh M. Marsh PhD[1*]

[1]Ludwig Boltzmann Institute for Lung Vascular Research, Graz, Austria. [2]The Brooke Laboratory, Academic Unit of Clinical and Experimental Sciences, Faculty of Medicine, University of Southampton, Southampton, United Kingdom.[3]National Institute for Health Research (NIHR) Southampton Respiratory Biomedical Research Unit, University Hospital Southampton NHS Foundation Trust, Southampton, United Kingdom. [4]Institute for Life Sciences, University of Southampton, Southampton, United Kingdom. [5]Institute of Experimental and Clinical Pharmacology, Medical University of Graz, Graz, Austria. [6] Department of Physiology, Medical University of Graz, Graz, Austria

Corresponding Author

Leigh Marsh PhD, Ludwig Boltzmann Institute for Lung Vascular Research, c/o ZMF, Stiftingtalstrasse 24, 8010 Graz, Austria. Leigh.marsh@lvr.lbg.ac.at

Supplementary Figure Legends

Supplementary Figure 1. Immunohistological negative control for p22phox in human lung tissue without primary antibody.

Supplementary Figure 2. Mouse treatment protocol

Mice were treated intra-nasally (i.n.) with a crude extract of HDM or PBS once a week over a six week period. Analysis was performed 72 hours after the last challenge.

Supplementary Figure 3. Control staining and western blotting for p22phox.

A. Expression of p22phox protein in lung homogenate from WT and p22phox KO mice. B. Immunohistological staining of p22phox in lungs samples from p22phox KO mice along with negative control without primary antibody (NGC). C. Negative control for the co-immunostaining for p22phox with cytokeratin/SMA with the omission of the primary antibodies. D. Immunofluorescent staining of p22phox in lungs from WT and P22phox KO mice

Supplementary Figure 4. Differential regulation of NOX enzymes and its subunits in PBS and HDM treated mice

mRNA Expression analysis of NADPH oxidases and subunits in lung homogenate samples of WT mice treated with PBS or HDM by real-time PCR. Tukey boxplots show medians, n = 8, *$p \leq 0.05$.

Supplementary Figure 5: HDM induced ROS production is diminished in presence of SOD

A. Changes in ROS production in single cell lung preparation from PBS and HDM mice treated with or without SOD as detected by A) H_2DCFDA and B) DHE fluorescence.

Supplementary Figure 6: Differential expression genes involved antioxidant of in p22phox KO and WT mice treated with HDM

mRNA expression in lung homogenate samples of p22phox KO and WT mice treated with HDM as determined by real-time PCR. Tukey boxplots show medians, n = 8, *$p \leq 0.05$.

Supplementary Figure 7: Immunoglobulin levels following HDM treatment

Serum levels of HDM-specific immunoglobulins in WT and KO mice following treatment with PBS or HDM treatment A) IgG1a, B) IgE and C) IgG2c. n = 7-8, *$p \leq 0.05$, **$p \leq 0.01$, ***$p \leq 0.001$.

Supplementary Figure 8. Inflammatory profiling in p22phox KO and WT mice treated with HDM

Flow cytometric analysis for inflammatory cells in mouse lung homogenate samples. Tukey boxplots show medians, n = 6-7, **p ≤ 0.01, ***p ≤ 0.001.

Supplementary Figure 9. Cytokines profiling in p22phox KO and WT mice treated with HDM

Expression analysis of inflammatory cytokines and chemokines in lung homogenate samples of p22phox KO and WT mice treated with PBS or HDM by real-time PCR. Tukey boxplots show medians, n = 4-8, **p ≤ 0.01, ***p ≤ 0.001.

Supplementary Figure 10.

Changes in ROS production in single cell lung homogenate treated with or without IL-13 as detected by A) H_2DCFDA and B) DHE fluorescence. C) Phospho STAT6 levels in mice trachea with and without exogenous treatment of H_2O_2

Supplementary Figure 11. Compendium of all complete western blot images contained within the manuscript

A) blots from Fig. 2D; B) blots from Fig. 7A, upper panel p22phox, lower panel aTubulin; C) blots from Fig. 7C, upper panel pSTAT6, lower panel aTubulin; D) blots from Supplementary Fig. 3A, upper panel p22phox, lower panel aTubulin; E) Uncropped blots from Supplementary Fig. 10C, upper panel pSTAT6, lower panel aTubulin.

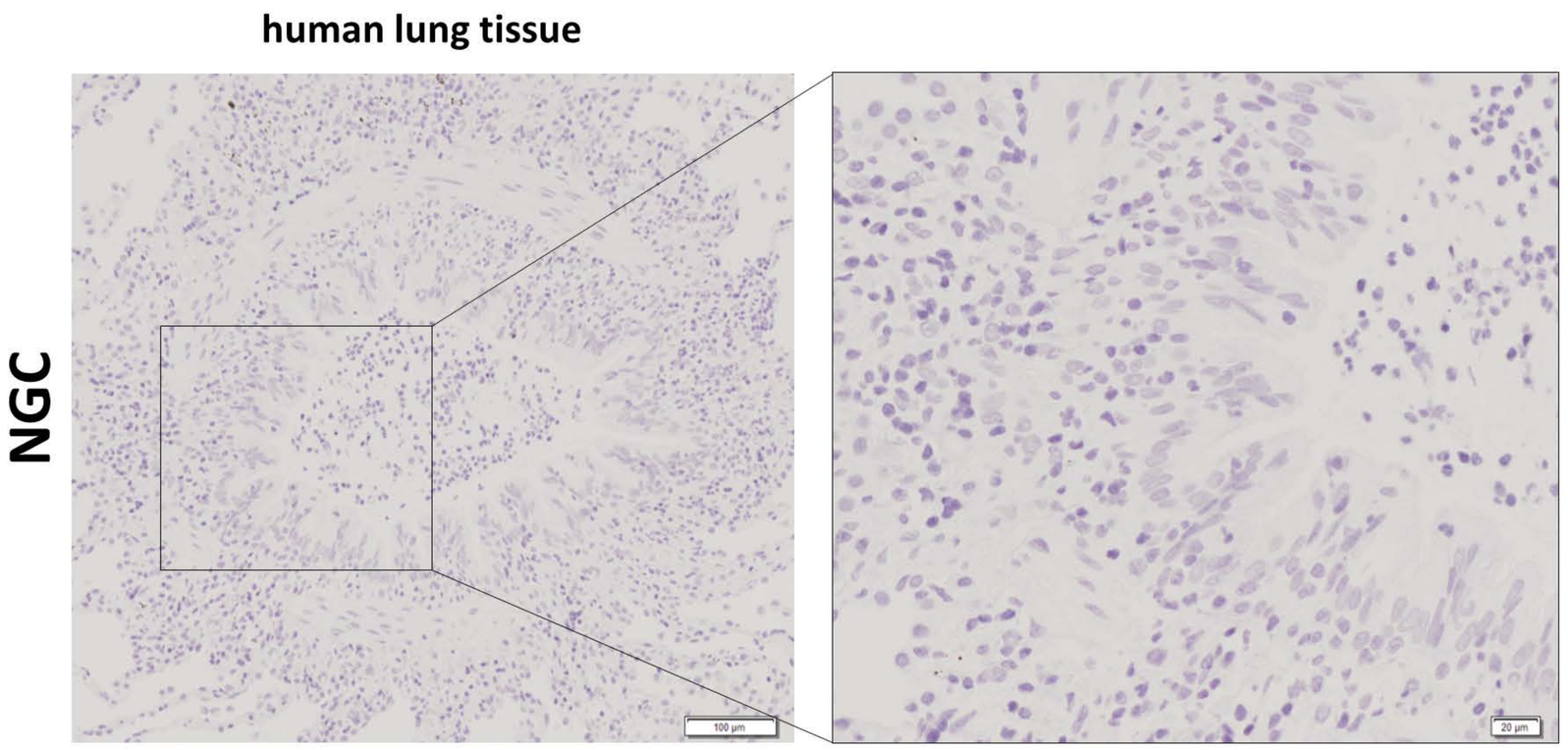

Supplementary Figure 1. Negative control (NHC) for p22phox immunohistochemistry in human lung tissue with the omission of the primary antibody (NGC).

Supplementary Figure 2. Mouse treatment protocol

Mice were treated intra-nasally (i.n.) with a crude extract of HDM or PBS once a week over a six week period. Analysis was performed 72 hours after the last challenge.

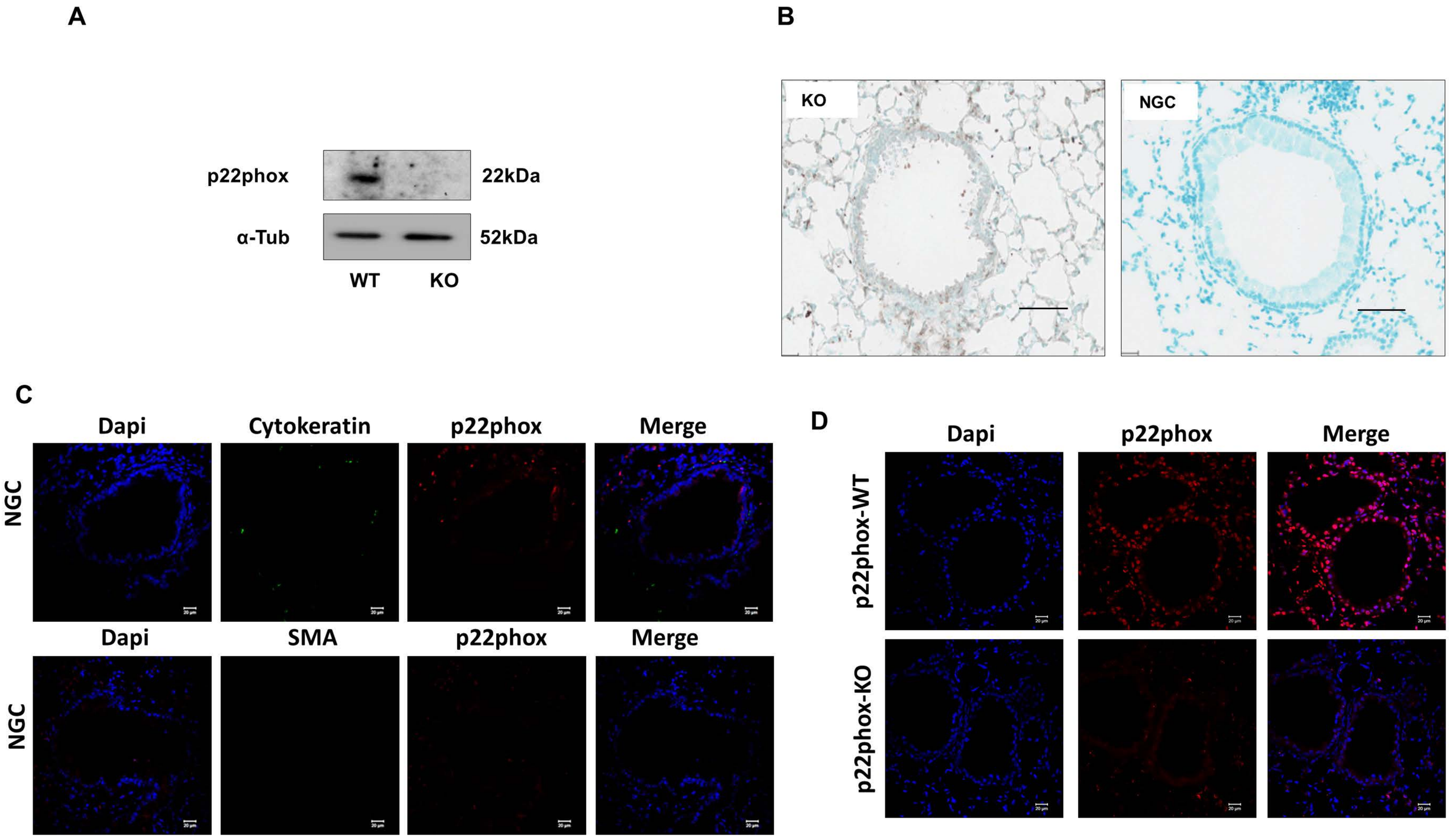

Supplementary Figure 3. Control stainings and western blotting for p22phox.

A. Expression of p22phox protein in lung homogenate from WT and p22phox KO mice. B. Immunohistological staining of p22phox in lungs samples from p22phox KO mice along with negative control without primary antibody (NGC). C. Negative control for the co-immunostaining for p22phox with cytokeratin/SMA with the omission of the primary antibodies. D. Immunofluorescent staining of p22phox in lungs from WT and P22phox KO mice

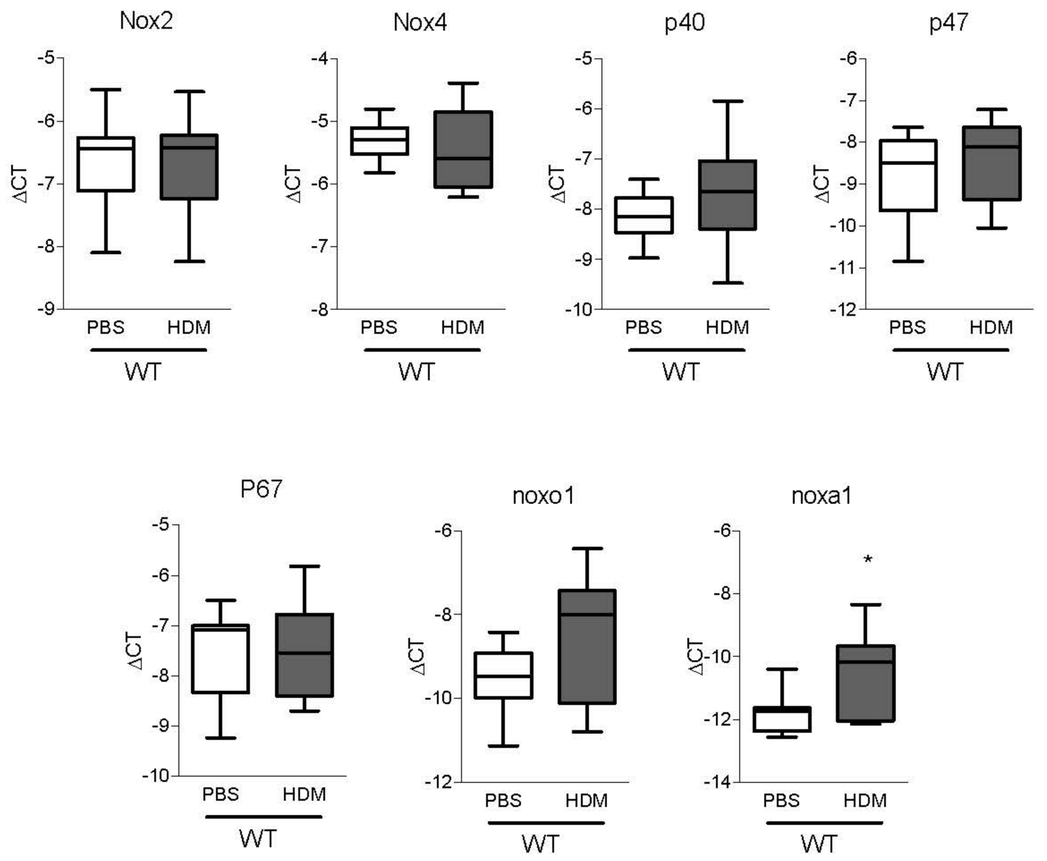

Supplementary Figure 4. Differential regulation of NOX enzymes and its subunits in PBS and HDM treated mice

mRNA Expression analysis of NADPH oxidases and subunits in lung homogenate samples of WT mice treated with PBS or HDM by real-time PCR. Tukey boxplots show medians, n = 8, *p ≤ 0.05.

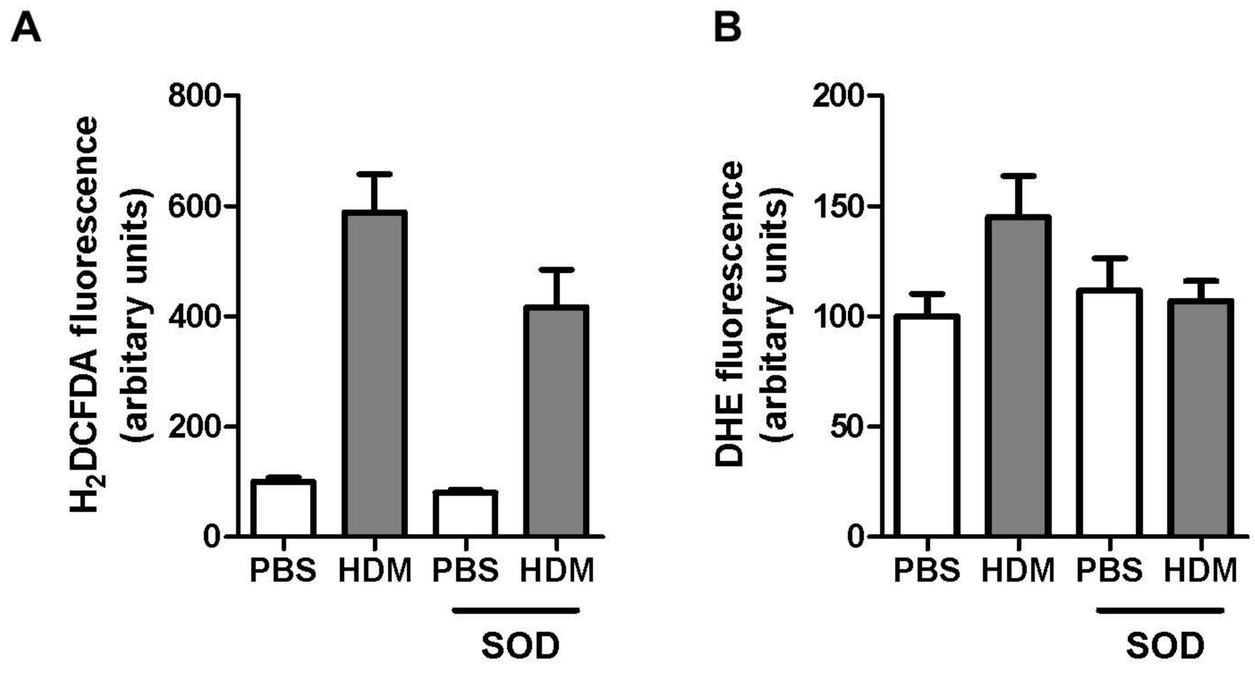

Supplementary Figure 5: HDM induced ROS production is diminished in presence of SOD

Changes in ROS production in single cell lung preparation from PBS/HDM treated mice with or without SOD as detected by A) H_2DCFDA B) DHE fluorescence for detection of ROS.

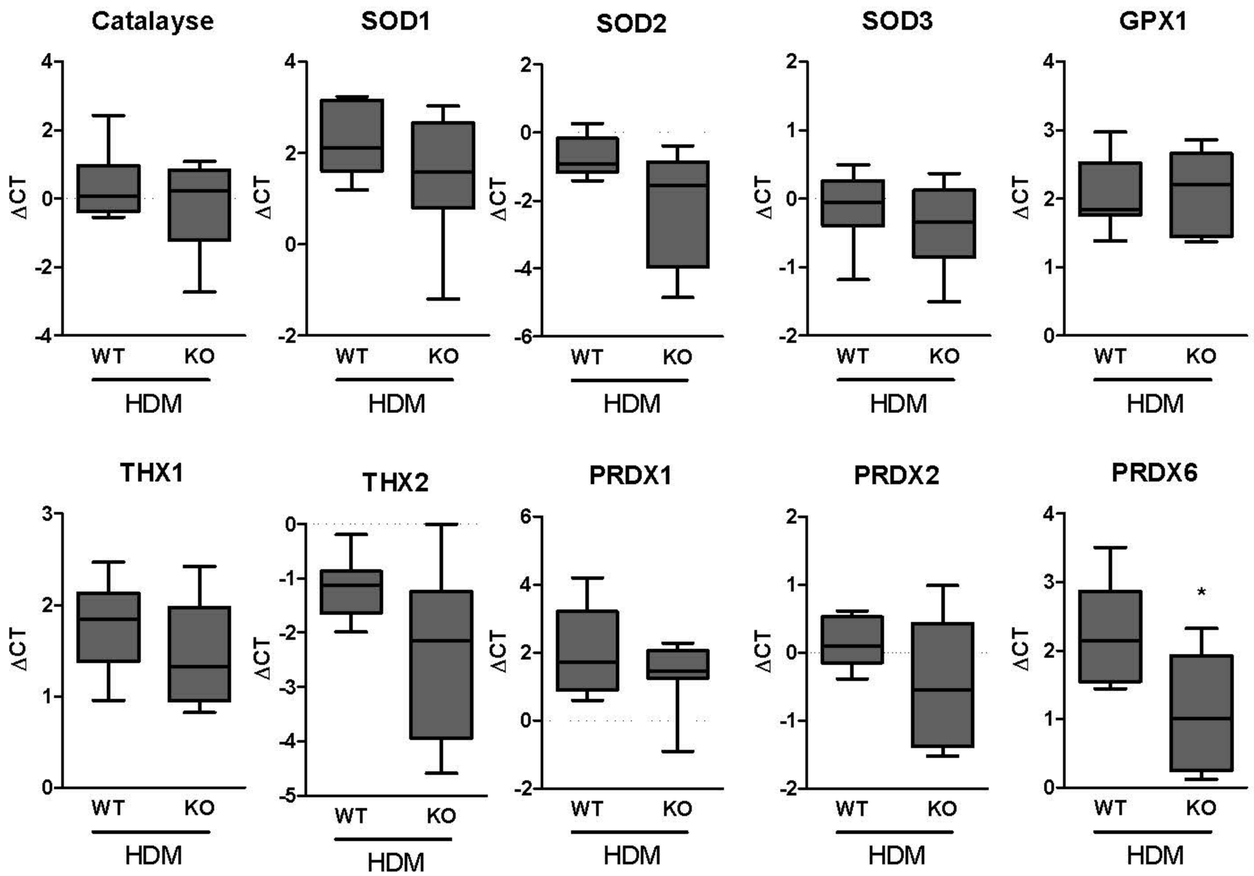

Supplementary Figure 6: Differential expression genes involved antioxidant of in p22phox KO and WT mice treated with HDM

mRNA expression in lung homogenate samples of p22phox KO and WT mice treated with HDM as determined by real-time PCR. Tukey boxplots show medians, n = 8, *p ≤ 0.05.

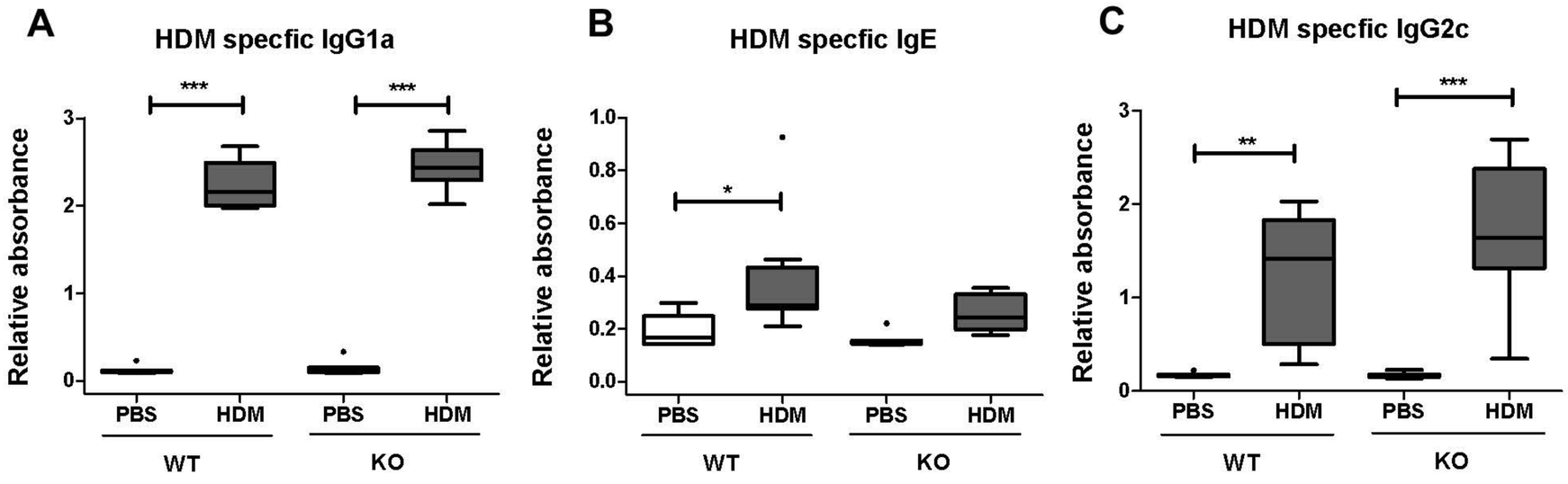

Supplementary Figure 7: Immunoglobulin levels following HDM treatment

Serum levels of HDM-specific immunoglobulins in WT and KO mice following treatment with PBS or HDM treatment A) IgG1a, B) IgE and C) IgG2c. n = 7-8, *p ≤ 0.05, **p ≤ 0.01, ***p ≤ 0.001.

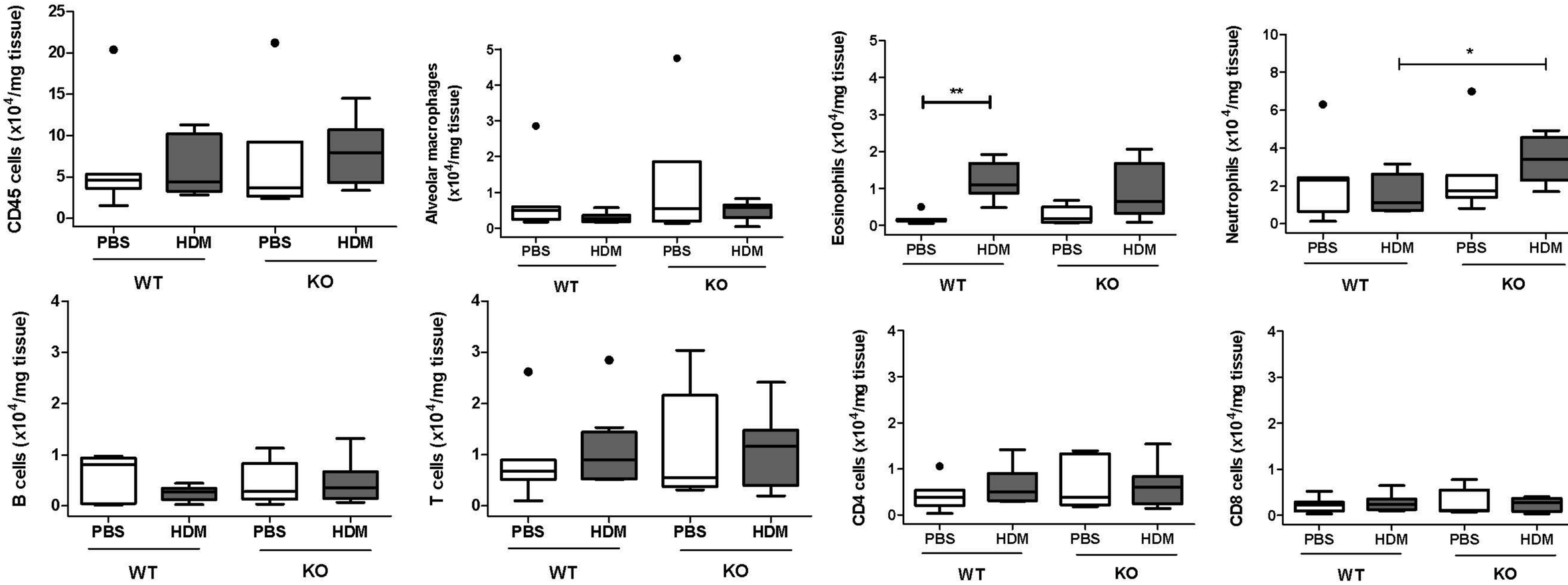

Supplementary Figure 8. Inflammatory profiling in p22phox KO and WT mice treated with HDM

Flow cytometric analysis for inflammatory cells in mouse lung homogenate samples. Tukey boxplots show medians, n = 6-7, **p ≤ 0.01, ***p ≤ 0.001.

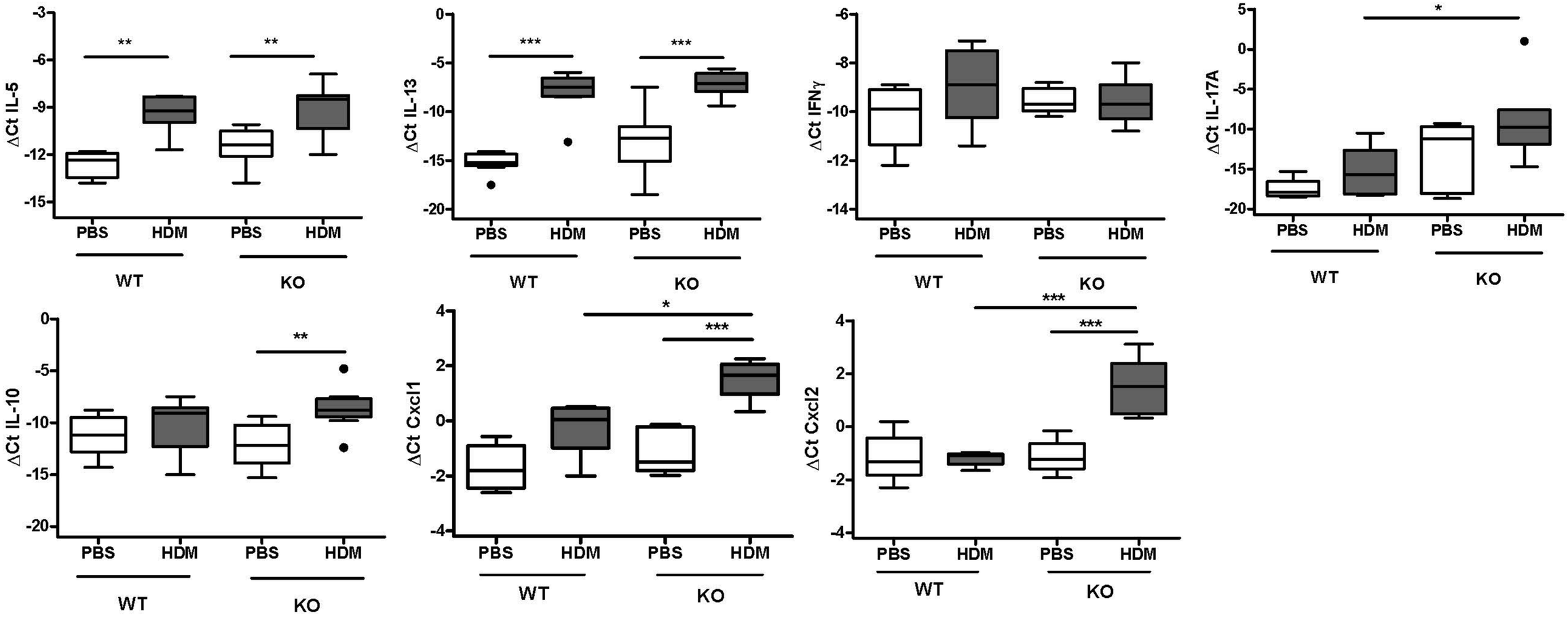

Supplementary Figure 9. Cytokine profiling in p22phox KO and WT mice treated with HDM

Expression analysis of inflammatory cytokines and chemokines in lung homogenate samples of p22phox KO and WT mice treated with PBS or HDM by real-time PCR. Tukey boxplots show medians, n = 4-8, **p ≤ 0.01, ***p ≤ 0.001.

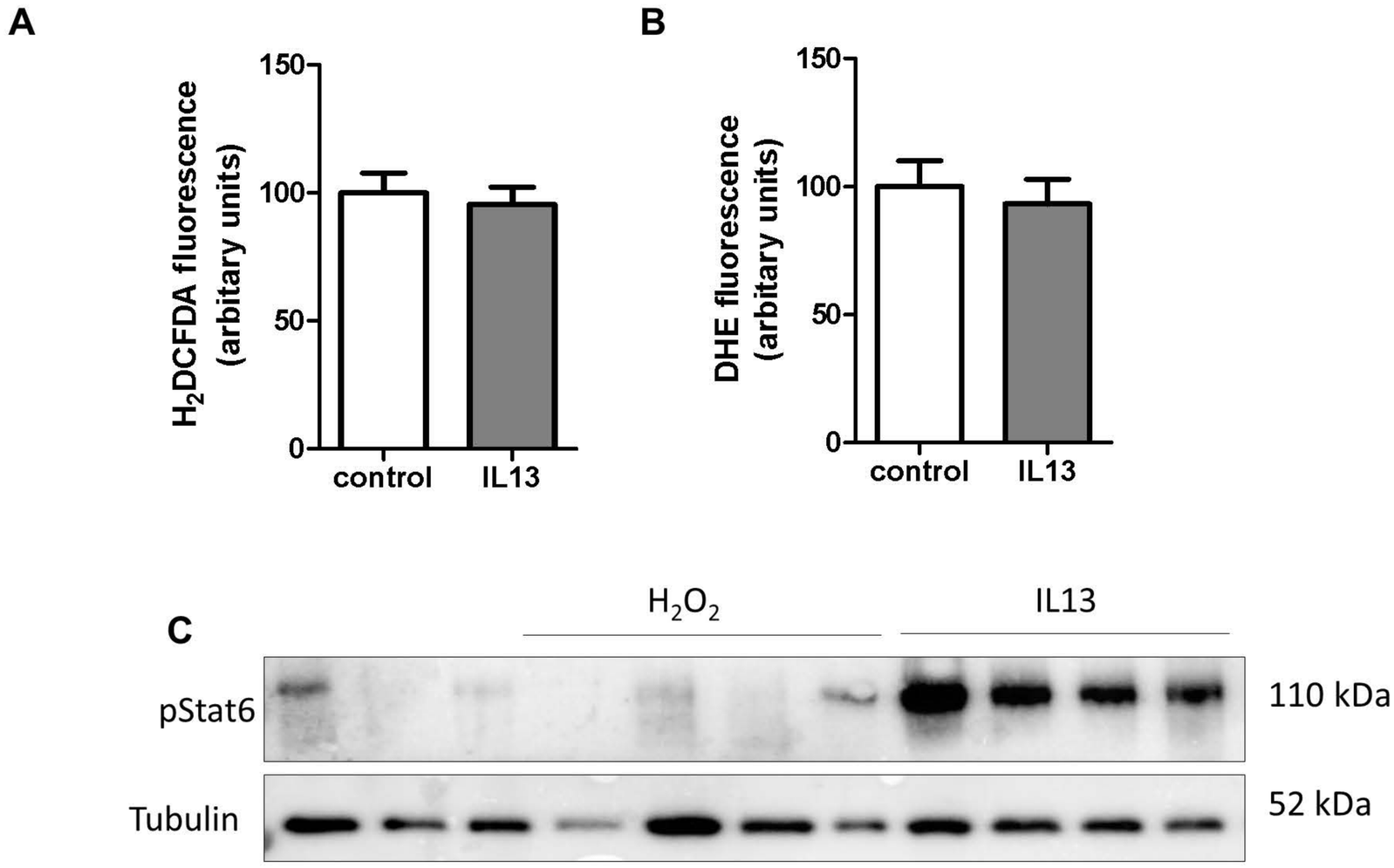

Supplementary Figure 10: Changes in ROS production in single cell lung homogenate treated with or without IL 13 as detected by A) H_2DCFDA and B) DHE fluorescence for detection of ROS. C) Phospho STAT6 levels in mice trachea with and without exogenous treatment of H_2O_2

Supplementary Figure 11